Paper No. 17

A SYNTHESIS OF UNSTEADY AERODYNAMIC EFFECTS INCLUDING STALL HYSTERISIS

by

T.S. BEDDOES
WESTLAND HELICOPTERS LIMITED

1. INTRODUCTION

A calculation procedure has been prepared with the primary objective of providing a practical method for incorporating unsteady section aerodynamic effects in the theoretical analysis of rotor aerodynamics. Factors involved in the approach to the formulation include reasonable computation time and complexity, the ability to handle arbitrary forcing functions in addition to harmonic terms and the inclusion of both unseparated and separated flow regimes. In the normal operating regime of the rotor, unsteady aerodynamic terms are of low magnitude and have been largely neglected. Operation near the flight boundary, in hover or forward flight implies a proximity to local stall and in this situation there is an increased sensitivity to small perturbations via the onset of transient separated flow.

The various sources of blade aerodynamic forcing are shown in Figure 1 which includes order of magnitude values for amplitude and frequency (or duration). Most of the large amplitude terms occur at the 1/rev. frequency. Those which involve blade response normally tend to cancel basic forcing terms. However, depending on the type of rotor, there may be some phase shift even in these terms and there remains a basic 1/rev. loading in forward flight. Higher harmonics are associated with bending and torsional response. The torsional amplitude at 5/rev. (nominal natural frequency) is omitted, under normal flight conditions there is very little response but at the flight boundary large transient excursions may be excited accompanied by low or negative damping. This source normally generates the control system and blade vibratory loads which impose the speed and load limitations of the rotor system as a whole. An exception to forcing of harmonic nature involves the encounter or proximity of discrete vortices embedded in the wake, these give rise to impulsive loadings which excite the higher natural frequencies.

Manoeuvring conditions change the relative geometry of the wake in such a manner that direct vortex encounter is provoked. The combination of all the above contributions can result in angle of attack changes of significant magnitude and short duration. When this occurs in the proximity of the stall the resulting force and moment characteristics may be quite different from those generated under quasi-static conditions, in fact, both the lift and pitching moment can be very much larger.

2. ATTACHED FLOW MODEL

When the higher frequencies are excited as by impulsive loadings the potential lift and, more particularly, the moment terms are no longer insignificant. These terms are normally derived as functions of the reduced frequency $\frac{\omega c}{2V}$ which, in the rotor environment is subject to a basic 1/rev. variation in the velocity term. We are also faced with a combination of different frequencies, amplitudes, phase differences and discontinuous changes in rotor forcing. Moreover, rotor loading calculations are performed commonly in a stepwise manner with the azimuth interval as an independent variable. These considerations lead to the logical choice of an indicial response (response to a stepwise

SOURCE	AMPLITUDE (DEG)	PERIOD (SEC)
CYCLIC PITCH	10 0	0 2
TORSIONAL DEFLECTIONS, 1/REV	1 5	0 2
TORSIONAL DEFLECTIONS, 2/REV	0·5	0 1
TORSIONAL DEFLECTIONS, 5/REV	—	0 04
FLAPWISE DEFLECTIONS, 1/REV	8·0	0·2
FLAPWISE DEFLECTIONS, 2/REV	3·0	0·1
FLAPWISE DEFLECTIONS, 3/REV	1 5	0·06
GROSS WAKE (MIDSPAN)	3 5	0 2
VORTEX PASSAGE	5·0	0·04

FIG.1. FORMS OF EXCITATION, POTENTIAL ANGLE OF ATTACK CHANGES.

$$C_L = C_{L_\alpha} \Delta\alpha \, \phi(S) = C_{L_\alpha} \alpha_E(S)$$

$$\phi(S) = 1 - A_1 e^{-b_1 s} - A_2 e^{-b_2 s}$$

FOR A TIMEWISE SAMPLED SYSTEM

$$\alpha_E(t) = \alpha_{(n=0)} + \sum_1^n \Delta\alpha_n - X_n - Y_n$$

WHERE

$$X_n = X_{(n-1)} e^{\frac{-2b_1 V \Delta t}{c}} + A_1 \Delta\alpha_n$$

$$Y_n = Y_{(n-1)} e^{\frac{-2b_2 V \Delta t}{c}} + A_2 \Delta\alpha_n$$

FIG.2. APPLICATION OF THE INDICIAL LIFT FUNCTION.

change in forcing) approach for the solution of time varying lift and moment. The classical solution is that of Wagner (see ref. 2) and the resulting indicial lift function $\phi(s)$ can be approximated in terms of exponential functions as shown in Figure 2. For application to the rotor problem the solution can be re-formulated for a timewise sampled solution, X_n and Y_n may be viewed as lift decrements decaying with time. For general motion, i.e. non-uniform downwash across the chord, the instantaneous angle of attack is replaced by the value of downwash at the $\frac{3}{4}$ chord. Thus, apart from this change, there is no distinction in the nature of the forcing. Additional lift and moment terms are derived (ref. 2) from apparent mass effects.

The Wagner function was derived for incompressible flow. In ref. 1 is shown the derivation of modified indicial lift functions for compressible flow. Ignoring the singularities near the origin which are associated with the apparent mass terms, Figure 3 shows both the compressible and incompressible indicial lift functions. It can be seen that it is possible to generalise the effects of compressibility for the range given by substituting $s(1-M^2)$ in the Wagner function modified by $\sqrt{1-M^2}$. This allows substitution of the modified indicial lift function in the simple sampled form of the analysis bearing in mind that Mach number is varying with time. The idealisation of $\phi_c(s)$. $\sqrt{1-M^2}$ allows substitution of the experimental value of the compressible lift curve slope when this is available and the equivalent in time of $s(1-M^2)$ as the sampling interval.

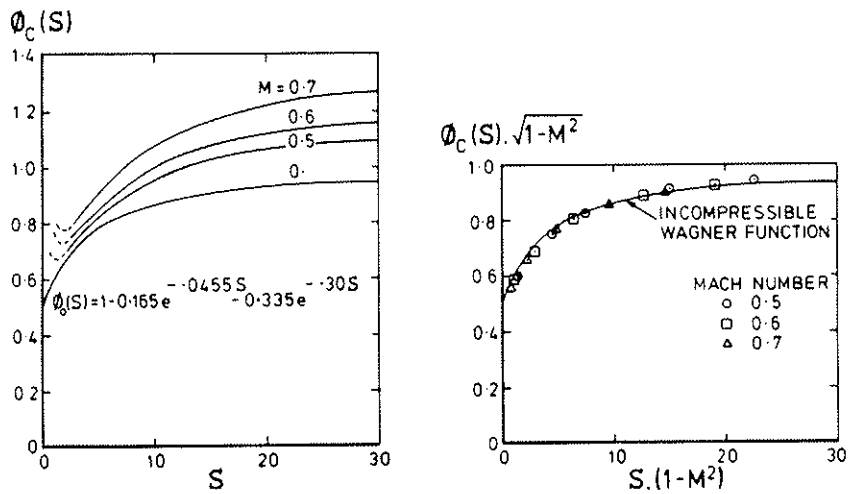

FIG.3. GENERALISATION OF THE INDICIAL LIFT FUNCTION.

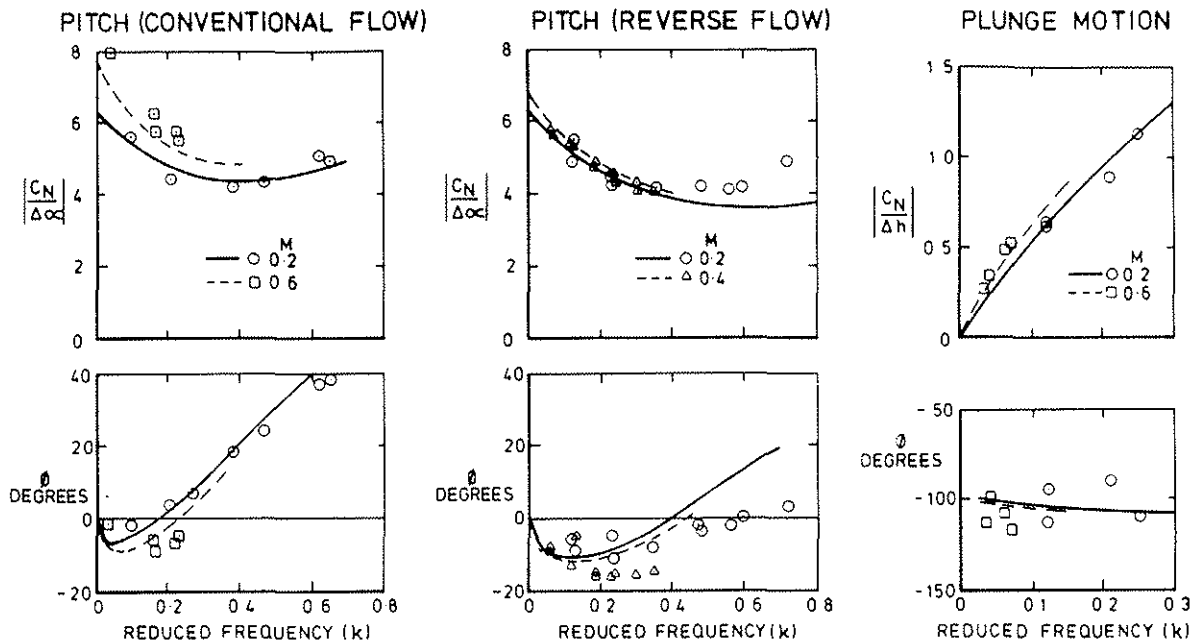

FIG.4. COMPARISON OF HARMONIC OSCILLATION TEST DATA WITH THEORY.

Pitching moment is implemented via the apparent mass terms as outlined in reference 2. For the compressible case, these terms in the lift expression become inappropriate (see reference 1). To preserve the simplicity of the model they are retained in a modified fashion, i.e. factored by $(1-M^2)$.

The model so far described is applicable only to attached flow conditions. To substantiate its validity it has been applied to the case of harmonically oscillating airfoils, using a stepwise solution, and the results compared with test data from references 3 through 5. Figure 4 shows this comparison in terms of the resulting amplitude and phase relationships in which the effect of Mach number is included for three different modes of motion, i.e. pitch for forward and reverse flow and pure plunge motion. Correlation is good with the exception of reverse flow at high reduced frequency.

3. DYNAMIC STALL MODEL

Representation of the separated flow regime is accomplished via an hypothesis of a physical model. This has been developed from observation of the large amount of experimental data produced in recent years, the main body of which is comprised of references 3 through 5. The main features of this model are shown in Figure 5. It is basically dependent on static characteristics which are of course in turn dependent, for a given profile, on Reynolds and Mach numbers, model surface condition and interference effects inherent in the configuration of the test rig, when appropriate. The static characteristics are idealised in a segmented fashion, the most critical feature is the break in the C_m vs α curve (α_1) which delimits the linear range. Beyond this point, under static conditions, the boundary layer can no longer withstand the adverse pressure gradients generated by increasing lift, the ensuing growth of separation subsequently limiting the maximum lift attainable. At some further, higher, angle of attack (α_2) the centre of pressure (c.p.) of the separated flow reaches a more or less stabilised value. In the intermediate range the c.p. is assumed to vary linearly with α. Lift characteristics from NACA test of an airfoil with forced separation at the leading edge are used to represent the condition at moderate angles of attack where the flow has failed to re-attach, for convenience a curve fit of $C_N = 1.1 \sin 3\alpha$ is used.

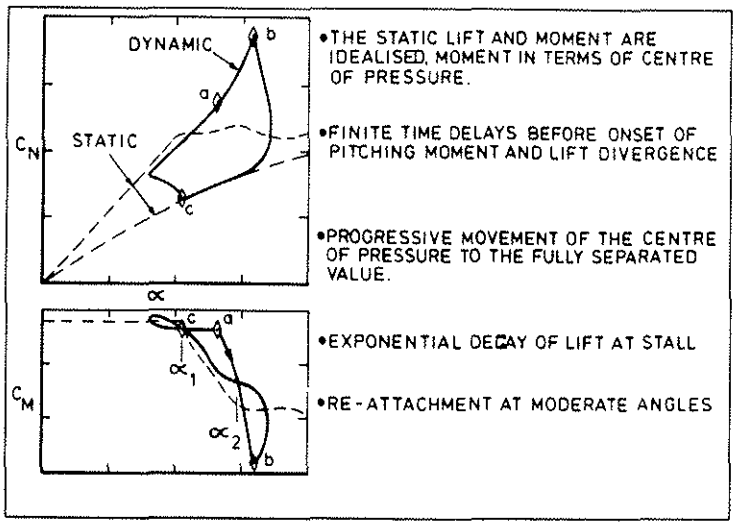

FIG.5. FEATURES OF THE DYNAMIC STALL MODEL.

NON DIMENSIONAL TIME = $\frac{\Delta t.V}{C}$

TIME DELAY:

	MEAN	STANDARD DEVIATION	SAMPLES
MOMENT BREAK	2·44	·49	142
LIFT BREAK	5·41	·61	123

RANGE OF TEST PARAMETERS:

REDUCED FREQUENCY	·04 — 0·67
MEAN ANGLE ~ DEGREES	2·5 — 20·0
AMPLITUDE ~ DEGREES	2·5 — 10·5
$\frac{\dot{\alpha}C}{2V}$ AT DIVERGENCE	-0·1 — +0·06
MACH NUMBER	0·2 — 0·6
NUMBER OF AIRFOILS	4
MODES OF MOTION	3

FIG.6. STATISTICAL ANALYSIS OF TIME DELAYS.

The most basic feature of the present model for dynamic stall are two essentially unique time delays for the onset of pitching moment and lift divergence. The consequence, in terms of angle of attack is shown in Figure 5. Point (a) illustrates the delay in the divergence of pitching moment. After a further delay (point b) the lift, which up to this time has been calculated on the basis of attached flow, decays according to a simple exponential function of time toward the fully separated value. As the angle of attack reduces below α_1, (point c) a process of re-attachment is initiated; using the separated value as an initial condition the lift change vs time is implemented using the same expression as for attached flow.

As the delays are a function of time rather than angle of attack, then, dependent on such parameters as mean angle, amplitude, frequency and velocity, for harmonic forcing the sequence of events described above will shift throughout a cycle expressed in terms of angle of attack. This results in considerable variation in the phasing of the pitching moment and lift breaks and the maximum values, with consequent implication on excitation and damping in the torsional mode.

From the sources noted above some 300 specific test cases have been examined and about 150 selected as demonstrating lift and/or moment divergence. From inspection of the time delays generated there appears, somewhat surprisingly, to be no significant dependence on the parameters of frequency, mean angle, amplitude, Mach number, mode of motion (pitch or plunge) or even the airfoil profile. The time delays do not appear to be sensitive to pitch rate, to a first order anyway, but it was observed that the sequence of events described appeared to speed up for decreasing values of angle of attack. For the model this has been accounted for simply by doubling the effective time interval whilst angle of attack is decreasing. The effect of this is included in the statistical analysis of the time delays presented in Figure 6.

Centre of pressure (c.p.) travel has been assumed to be a function of both angle of attack and time. Prior to the expiry of the time delay no change in c.p. is permitted. Subsequently, the timewise variation in response to a step change in c.p. is shown in Figure 7. The basic function is analogous to a second order lag, expressed in terms of the Laplace operator s in the Figure. It is implemented in the same manner as the indicial lift function. The net effect is to simulate transition from the c.p. corresponding to attached flow to the c.p. for separated or partially separated flow in the time period between the pitching moment and lift divergence. Additionally it introduces a lag in

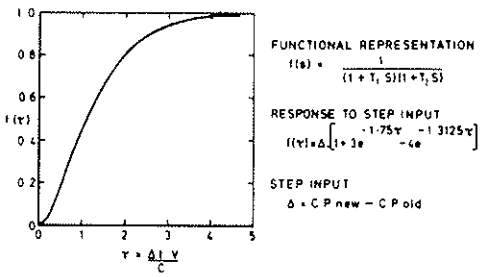

FIG.7. CENTRE OF PRESSURE TRAVEL.

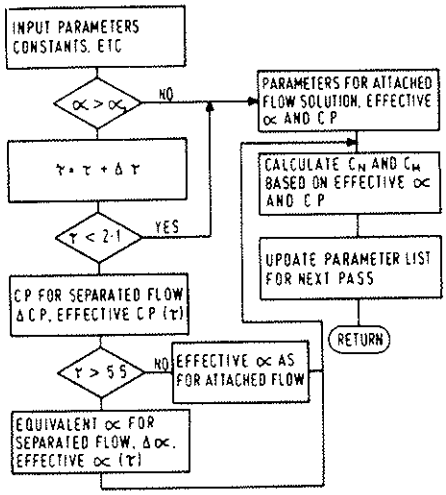

FIG.8. SIMPLIFIED FLOW DIAGRAM FOR CALCULATION OF NORMAL FORCE AND PITCHING MOMENT.

c.p. movement under separated conditions. During this time period an increase in C_N above the potential value has been observed, this can amount to as much as 15%. It may be attributed to the expanding pressure wave associated with the chordwise travel of the shed vortex, the peak pressure being a function of the initial circulation.

The above procedure has been programmed as a subroutine for inclusion in overall rotor airloads analysis. It has been kept as simple and efficient as possible and currently uses only about $\frac{1}{2}$ millisec (IBM 370/155) per step. A simplified flow diagram is shown in Figure 8. Input parameters comprise the independent variables, data from the prior step and the idealised airfoil data at the appropriate Mach number. If the angle of attack is less than α_1, or the non-dimensional time (τ) is less than that for pitching moment divergence (τ_1) then lift and moment are calculated as for attached flow. If τ is greater than τ_1 then the c.p. for separated flow and the appropriate time dependent value are calculated. Depending on whether τ is less than or greater than the value for lift divergence the effective angle of attack is calculated for either attached or separated conditions with the appropriate time dependence. On the basis of the effective angle of attack and c.p. the resulting normal force and pitching moment are calculated and the parameter list updated for the next pass.

4. EVALUATION AND COMPARISON WITH TEST

By far the largest available body of test data comprise refs. 3 through 5. These tests were performed by Vertol under contract to the U.S. Army. They cover several airfoils and modes of excitation, all of which, however, are harmonic. It has been stressed that the theoretical model has been formulated to handle forcing of an arbitrary sampled nature, thus the application to harmonic motion is a particular case. Correlation of the method has been performed with a number of cases from the above references and some examples are shown to illustrate features of the model.

Figure 9 shows how the relation between pitching moment and lift divergence time-delays influence the damping and maximum C_M. Considering each cycle in turn, the mean angle of attack increases consecutively. The first shows only very limited separation, it is sufficient, however, to introduce a small loop of negative damping which partially offsets the basic potential value. The second cycle shows earlier C_M divergence which increases the loop of negative damping reducing the overall value to close to zero. Further increase of mean angle

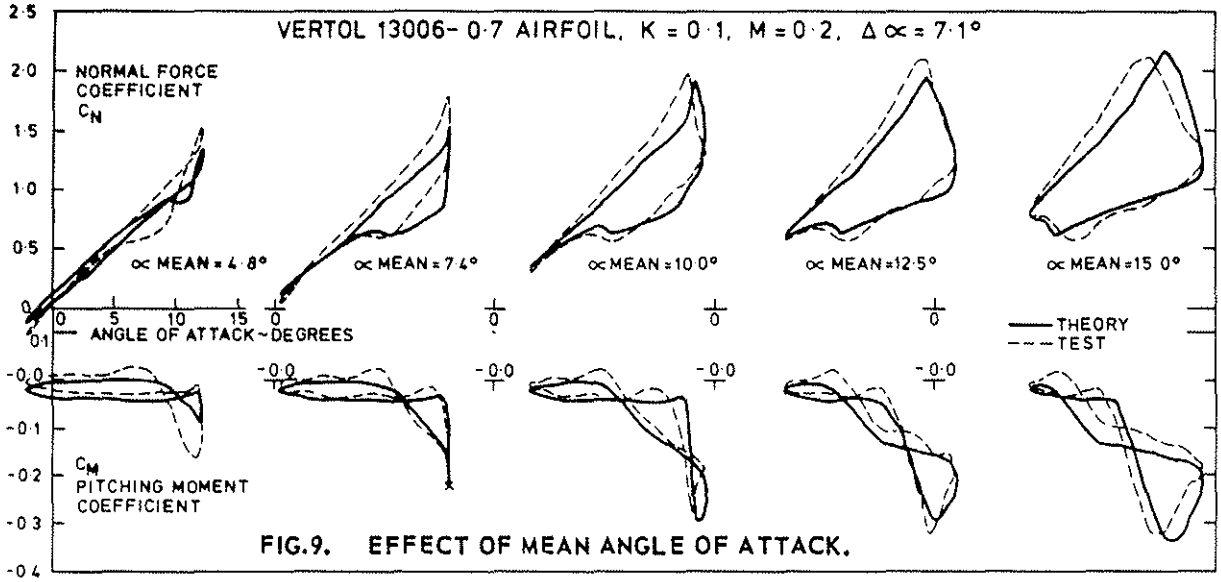

FIG.9. EFFECT OF MEAN ANGLE OF ATTACK.

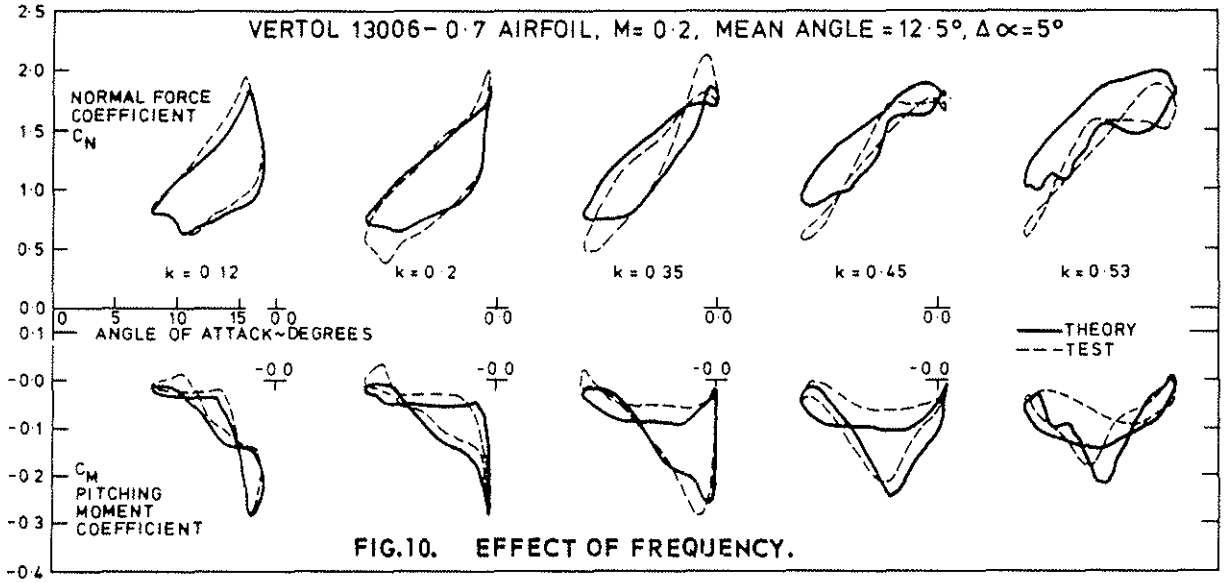

FIG.10. EFFECT OF FREQUENCY.

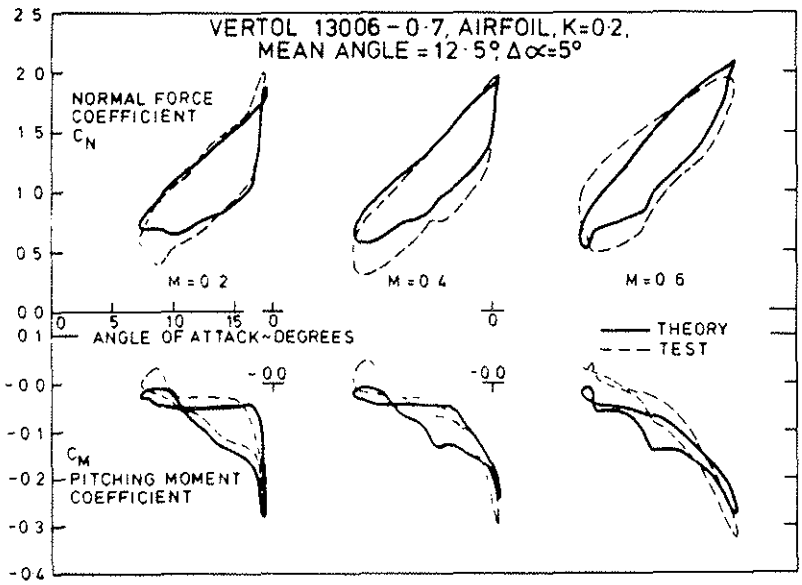

FIG.11. EFFECT OF MACH NUMBER AT CONSTANT REDUCED FREQUENCY

introduces an extra loop of positive damping, this is due to the c.p. having reached the fully separated value before the end of the cycle. Maximum pitching moment is now a function of C_{Lmax} which occurs earlier in the cycle and thus offsets the effect of the increasing mean angle.

Figure 10 shows how increasing frequency can allow more of the cycle to be completed before the onset of separation effects. In this particular case, it has the effect of initially driving the damping to more negative values and then subsequently in the direction of positive damping. The maximum values of pitching moment still occur at the point of lift divergence which, at the higher frequencies, is delayed to lower angles in the return part of the cycle, thus maximum C_M is no longer a function of the maximum lift. These data appear to show a delay in re-attachment at high frequency.

The effect of Mach number is shown in Figure 11. A constant value of reduced frequency is used to illustrate that exceptionally large values of normal force may be achieved at high Mach number. If a constant frequency were used for the comparison, the effect of the decrease in reduced frequency as Mach number increased would dominate the comparison and show a reduction in the maximum lift. The progressively earlier break in pitching moment is due to the influence of the static characteristics.

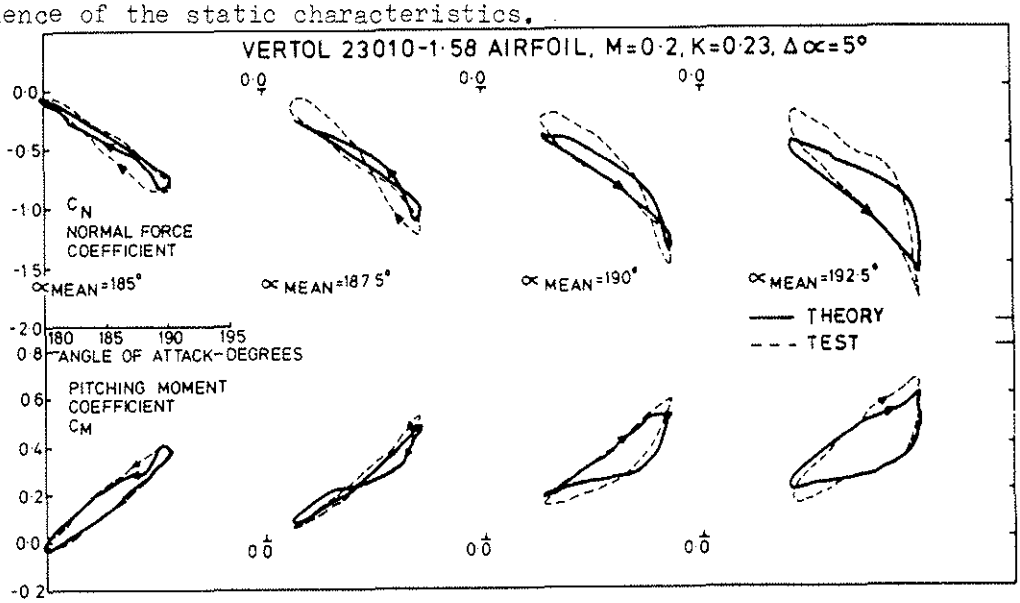

FIG.12. CHARACTERISTICS IN REVERSE FLOW.

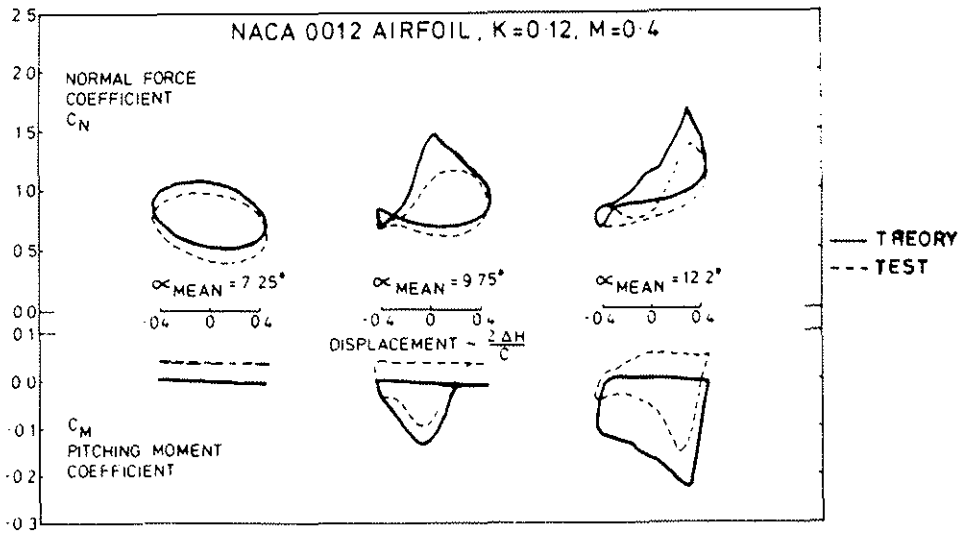

FIG.13. REPRESENTATION OF PLUNGE MOTION.

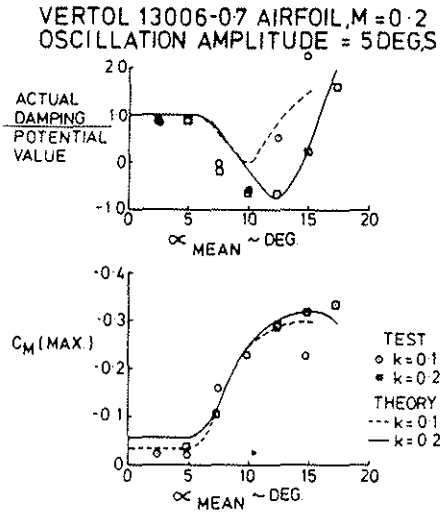

FIG.14. VARIATION OF DAMPING AND MAXIMUM PITCHING MOMENT.

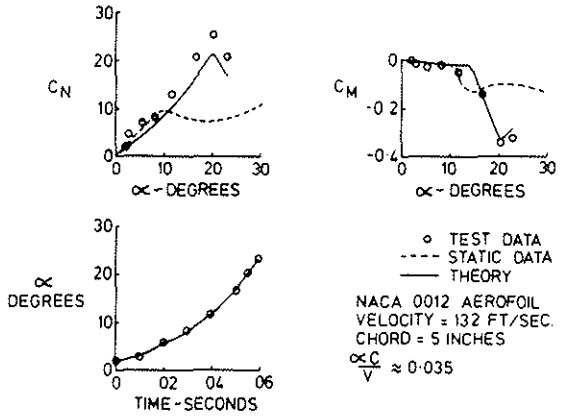

FIG.15. RESPONSE TO A RAMP INPUT.

That the model is equally applicable in reverse flow is shown by Figure 12. Large pitching moments are generated under attached flow conditions by the offset of the aerodynamic centre from the pitch and moment axis. Separation has the effect of reducing this offset as well as changing the shape of the loop. The high values of C_N are noteworthy. These results are particularly encouraging if the condition of reverse flow is viewed as a rather extreme modification of the thickness distribution.

Apart from the influence on downwash at the $\frac{3}{4}$ chord point and on virtual mass terms, no distinction is made between pitch and plunge motion in the model. Figure 13 shows a comparison of results for plunge motion with increasing mean angle. Shift of the test values of pitching moment for unseparated flow occurs somewhat randomly in the data and is not considered significant. Pitching moments are negligible for this mode when the flow is attached. $C_{L_{max}}$ is over-estimated for these cases which utilise the same section data as for the pitching mode. Modification to the rig in the form of end plates introduced some flow separation problems and may have resulted in some change to the section data. With the onset of separation effects, the maximum lift and moment values are achieved in a manner corresponding to that for pitch motion.

Following excitation of the torsional natural frequency, the damping of this mode is of prime concern. Figure 14 shows a comparison of both the maximum pitching moment and relative damping for harmonic pitch oscillation. Progression is shown from positive damping (potential solution) to negative values and back to positive at high mean angles. The mechanism of these changes is shown in Figure 9. Zero damping is the result of the combination of positive and negative loops and consequently it is very sensitive to small deviations in pitching moment. The re-attachment and return part of the cycle shows the most variation, an example, presented in reference 4, in four successive cycles shows a variation in damping ratio from zero to -0.8. Good matching of maximum pitching moment reinforces attribution of the discrepancy to this part of the cycle. Due to the non-linearity of the mechanism, the region of low and negative damping is a function of amplitude.

To illustrate application of the model to non-harmonic forcing, Figure 15 shows the response to a ramp input. The experimental data were taken from reference 6 and demonstrate the type of build up of angle of attack with time that might be associated with the proximity of a discrete vortex passage.

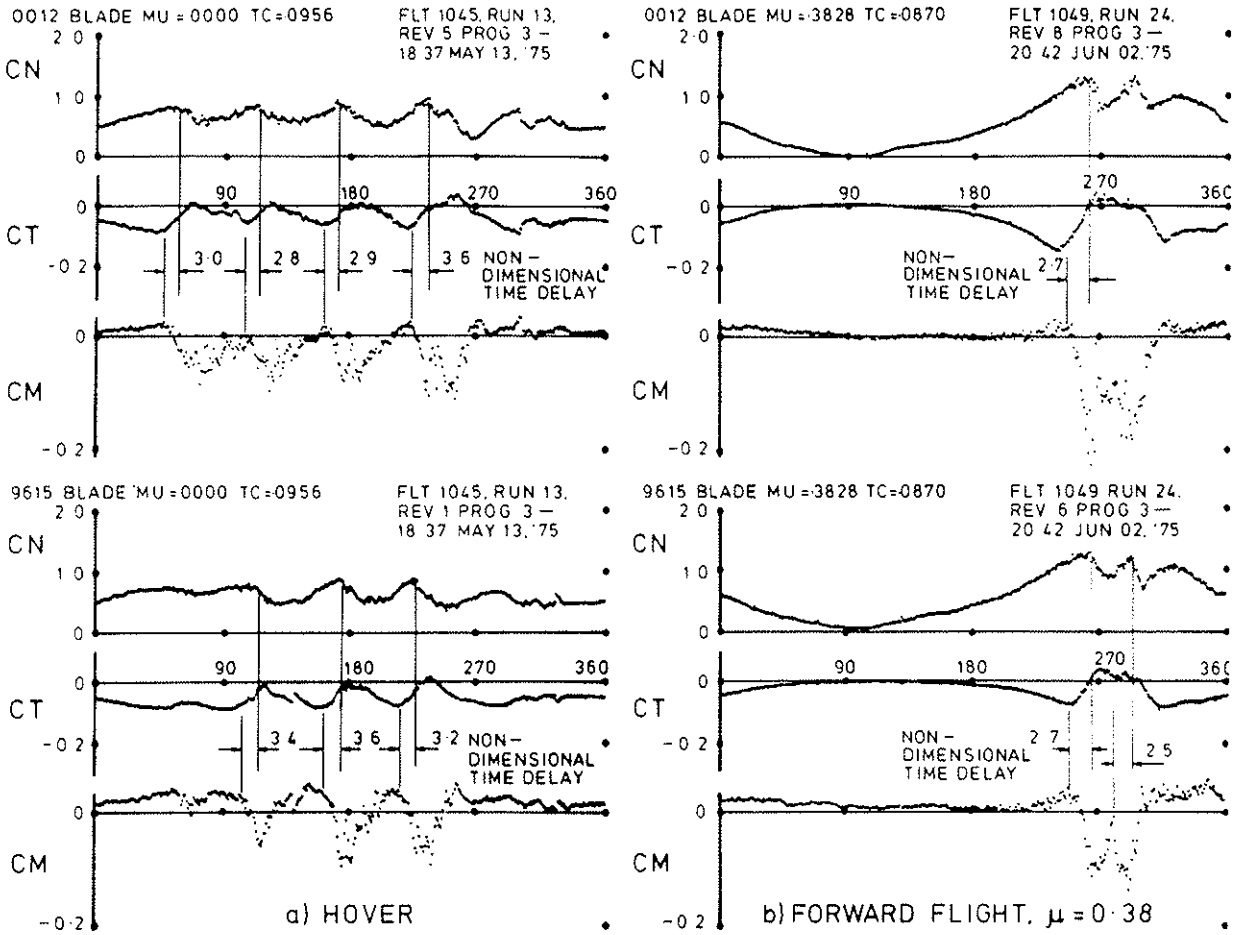

FIG.16. FLIGHT MEASUREMENTS OF THE TIME DELAY BETWEEN PITCHING MOMENT AND LIFT DIVERGENCE.

Some flight research has been performed recently at R.A.E. Bedford to investigate section characteristics in the region of the flight boundary. Pressure plotted airfoil gloves provide time history data of normal and chordwise forces and pitching moment; a description of these experiments has been presented in reference 7. Some preliminary data for two airfoil sections in hover and forward flight are shown in Figure 16. All the cases shown demonstrate large torsional moments and, in the case of hover, some instability. They are used to illustrate the non-dimensional time delay between pitching moment and lift divergence which, from the analysis of wind tunnel harmonic data, should be of the order of 3.0 with a standard deviation of about 0.6, experimental values are shown in the figure. The hover case demonstrates excitation of a slightly divergent oscillation at the torsional natural frequency and involves cycles of separation and re-attachment. The forward flight case involves separation on the retreating blade at a lower local Mach number and consequently higher C_N, this is followed by the passage of a tip vortex which triggers a repeated separation. The combination of these two events creates a sizeable torsional impulse which is transmitted to the control system. It can be observed that for the forward flight case, the azimuth interval involved is greater than for the hover. This is due to the local velocity term in the non-dimensional time delay and, in conjunction with the other demonstrated characteristics, would appear to substantiate application of the theoretical model to the full scale rotor environment.

5. CONCLUSIONS

A relatively simple computational model has been constructed for the synthesis of unsteady aerodynamics. It is based on a physical model for dynamic stall which has sufficient generality to be applicable to all airfoils and modes of excitation. As a result, it may be used to predict behaviour under conditions that have not been simulated under test and, being based on static airfoil characteristics, it may be used to predict changes in dynamic behaviour resulting from design or operational modifications to the profile. It is intended for engineering application, in particular, the investigation of rotor airloads and flight boundaries. Consequently, computational requirements have been minimised, stepwise sampling has been used to conform to conventional methods of rotor analysis and encompass a combination of forcing terms. Continuity is maintained in the timewise variation of attached and separated flow conditions and the large normal force and pitching moments demonstrated in wind tunnel tests are reproduced together with their relative phasing. Correlation has been demonstrated with a range of wind tunnel and flight experiments.

6. REFERENCES

1. R.L. Bisplinghoff, H. Ashley, R.L. Halfman, Aeroelasticity. Addison-Wesley (1957).
2. Y.C. Fung, An Introduction to the Theory of Aeroelasticity. Wiley & Sons Inc. (1955).
3. J. Liiva et al., Two Dimensional Tests of Airfoils Oscillating near Stall. USAAVLABS TR68-13 (1968).
4. L. Gray et al., Wind Tunnel Tests of Thin Airfoils Oscillating near Stall. USAAVLABS TR68-89 (1969).
5. L. Gray et al., Wind Tunnel Investigation of Airfoils Oscillating in Reverse Flow. USAAVLABS TR70-4 (1970).
6. N.D. Ham, M.S. Garelick, Dynamic Stall Considerations in Helicopter Rotors. Journal of the American Helicopter Society, April 1968.
7. P. Brotherhood, Flight Measurements of Helicopter Rotor Aerofoil Characteristics and Some Comparisons with Two-Dimensional Wind Tunnel Results. Paper presented at the AGARD Symposium on 'Flight/Ground Testing Facilities Correlations' at Modane, France, June 1975.

7. NOTATION

b_1, b_2	constants
c	airfoil chord
C_N	normal force coefficient
C_M	pitching moment coefficient
h	heave displacement, positive up
k	reduced frequency, $\frac{\omega c}{2V}$
M	Mach number
s	streamwise distance, semichords
t	time, seconds
V	local airstream relative velocity, ft/sec
α	angle of attack
τ	non-dimensional time $\frac{t.V}{c}$
ϕ	phase angle
$\phi(s)$	indicial lift function
ω	frequency, radians/sec